Astron. Astrophys. 334, 646–658 (1998)

ASTRONOMY AND ASTROPHYSICS

Molecular gas in the Galactic center region

III. Probing shocks in molecular cores⋆

S. Hüttemeister[1,2], G. Dahmen[3,4], R. Mauersberger[5], C. Henkel[4], T.L. Wilson[4,6], and J. Martín-Pintado[7]

[1] Radioastronomisches Institut der Universität Bonn, Auf dem Hügel 71, D-53121 Bonn, Germany
[2] Harvard-Smithsonian Center for Astrophysics, 60 Garden Street, Cambridge, MA 02138, USA
[3] Physics Department, Queen Mary & Westfield College, University of London, Mile End Road, London E1 4NS, UK
[4] Max-Planck-Institut für Radioastronomie, Auf dem Hügel 69, D-53121 Bonn, Germany
[5] Steward Observatory, The University of Arizona, Tucson, AZ 85721, USA
[6] Submillimeter Telescope Observatory, The University of Arizona, Tucson, AZ 85721, USA
[7] Centro Astronómico de Yebes, Apartado 148, E-19080 Guadalajara, Spain

Received 1 December1997 / Accepted 24 February 1998

Abstract. Multiline observations of $C^{18}O$ and SiO isotopomers toward 33 molecular peaks in the Galactic center region, taken at the SEST, JCMT and HHT telescopes, are presented. The $C^{18}O$ presumably traces the total H_2 column density, while the SiO traces gas affected by shocks and high temperature chemistry. The $J = 2 \rightarrow 1$ line of SiO is seen only in few regions of the Galactic disk. This line is easily detected in all Galactic center sources observed. A comparison of the strength of the rare isotopomers ^{29}SiO and ^{30}SiO to the strength of the main isotopomer ^{28}SiO implies that the $J = 2 \rightarrow 1$ transition of ^{28}SiO is optically thick. The $^{29}Si/^{30}Si$ isotope ratio of 1.6 in the Galactic center clouds is consistent with the terrestrial value. Large Velocity Gradient models show that the dense component ($n_{H_2} \geq 10^4\,cm^{-3}$) in typical molecular cores in the Galactic center is cool ($T_{kin} \approx 25\,K$), contrary to what is usually found in Giant Molecular Clouds in the disk, where the densest cores are the hottest. High kinetic temperatures, $> 100\,K$, known to exist from NH_3 studies, are only present at lower gas densities of a few $10^3\,cm^{-3}$, where SiO is highly subthermally excited. Assuming that $C^{18}O$ traces all of the molecular gas, it is found that in all cases but one, SiO emission is compatible with arising in gas at higher density that is (presently) relatively cool. The relative abundance of SiO is typically 10^{-9}, but differs significantly between individual sources. It shows a dependence on the position of the source within the Galactic center region. High abundances are found in those regions for which bar potential models predict a high likelihood for cloud-cloud collisions. These results can be used to relate the amount of gas that has encountered shocks within the last $\sim 10^6$ years to the large scale kinematics in the inner ~ 500 pc of the Galaxy.

Key words: ISM: clouds – ISM: molecules – ISM: structure – Galaxy: center – radio Lines: ISM

1. Introduction

The molecular environment in the inner $\sim 8^\circ$ of the Galaxy differs drastically from that in the Galactic disk. Large scale surveys of CO isotopomers (e.g. Bally et al. 1987, Heiligman 1987, Jackson et al. 1996, Dahmen et al. 1997a (Paper I), Bitran et al. 1997) show that the cloud and the intercloud medium in the gaseous bulge of the Milky Way are molecular. The gas is characterized by large linewidths, indicating a high degree of turbulence. As shown by Dahmen et al. 1998 (Paper II), there is no simple relationship between CO line intensities and H_2 column densities and thus no global $N(H_2)/I(CO)$ conversion factor.

Except for a few extraordinary regions such as Sgr A and Sgr B2, little evidence for ongoing massive star formation in Galactic center Giant Molecular Clouds (GMCs) is found, as is demonstrated by a general lack of strong FIR or radio continuum point sources associated with these clouds (Odenwald & Fazio 1984, Güsten 1989). Ambient dust temperatures are fairly low at $T_d \sim 25 - 30\,K$ (e.g. Cox & Laurijs 1989). Based on ISO data, this is also a typical T_d in the sources studied in this paper.

In the Galactic disk, quasithermal SiO emission is tightly correlated with high temperature regions (e.g. Ziurys et al. 1989). A close association with outflows strongly suggests that grain disruption by shocks is the major mechanism for releasing SiO into the gas phase (Martín-Pintado et al. 1992), although high temperature gas phase chemistry (Langer & Glassgold 1990) may play a minor role. In the Galactic center region, SiO is much more widespread (see e.g. the survey in the $J = 1 \rightarrow 0$

Send offprint requests to: S. Hüttemeister, RAIUB

⋆ Based on observations obtained at the Swedish-ESO Submillimeter Telescope (SEST, Project C-0518, 1996), the James Clark Maxwell Telescope (JCMT, operated by the Joint Astronomy Centre on behalf of the Particle Physics and Astronomy Research Council of the United Kingdom, the Netherlands Organisation for Scientific Research, and the National Research Council of Canada) and the Heinrich-Hertz-Telescope (HHT, operated by the the Submillimeter Telescope Observatory).

transition by Martín-Pintado et al. 1997), which was interpreted as evidence for large scale or ubiquitous (fast) shocks.

In this paper, $C^{18}O$ and SiO data are presented for molecular cloud cores of the Bally et al. (1987) CS survey. Our measurements allow to (1) trace the H_2 column density, (2) determine or constrain density and temperature structure, (3) estimate SiO abundances and (4) obtain information about silicon isotope ratios. Since our sources are selected on the basis of their intensity in CS, a general high density tracer, the sample is not a priori biased toward strong SiO emission.

NH_3 data (Hüttemeister et al. 1993b) show that at least two phases of different kinetic temperatures are present within all cloud cores without massive star formation: A cool component with $T_{\rm kin}$ of 20 – 30 K, close to the temperature of the dust in the Galactic center and a warm component with $T_{\rm kin} \geq 120$ K. $T_{\rm kin} \sim 75$ K is considered by many authors, (e.g. the reviews by Morris & Serabyn 1996, Mezger et al. 1996) as 'typical'. This is, however, just the average over the hot and cool component and has no meaning as a distinct physical component.

A major aim of this study is to determine the physical parameters, distribution and origin of these phases and to decide which of them, cool or warm, is associated with the bulk of the SiO emission.

2. Observations

The observations of the $J = 1 \rightarrow 0$ and $2 \rightarrow 1$ transitions of $C^{18}O$ and the $J = 2 \rightarrow 1$ transition of ^{28}SiO, ^{29}SiO and ^{30}SiO were carried out at the Swedish-ESO Submillimetre Telescope (SEST) at La Silla (Chile). All $C^{18}O(3 \rightarrow 2)$ data were taken at the James Clark Maxwell Telescope (JCMT) on Mauna Kea, (Hawaii), where we also obtained some $^{28}SiO(5 \rightarrow 4)$ and $C^{18}O(2 \rightarrow 1)$ measurements for calibration purposes. Finally, the $(5 \rightarrow 4)$ transition of ^{28}SiO was measured at the Heinrich Hertz Telescope (HHT) on Mt. Graham (Arizona). Table 1 summarizes the observations, including line frequencies, telescope parameters, receivers and spectrometers used and typical system temperatures. A telescope beamsize of 46″ corresponds to 1.9 pc at a distance of the Galactic center of 8.5 kpc.

Typically, the telescope pointing was checked every three hours. At SEST, two strong SiO masers close to the Galactic center, AH Sco and VX Sgr, were measured. At the JCMT, the pointing was done using five-point continuum maps on NGC 6334 I. At the HHT, continuum cross scans on Sgr B2 were used. At SEST and JCMT, the pointing accuracy was always better than 5″. At the HHT, the accuracy was always better than 10″ and usually 5″.

At all telescopes, calibration was done with the standard chopper wheel method, giving temperatures on the T_A^* scale. These were converted to $T_{\rm MB}$, the main beam brightness temperature (see, e.g., Downes 1989 and Rohlfs & Wilson 1996 for definitions), using the main beam efficiencies, $\eta_{\rm MB}$, listed in Table 1.

To account for structure in our extended sources, we mapped the beam used to measure the $C^{18}O(1 \rightarrow 0)$ line in the $(2 \rightarrow 1)$ and $(3 \rightarrow 2)$ transitions. Due to time restrictions, this was not possible for the $SiO(5 \rightarrow 4)$ line observed at the HHT. From maps obtained at the JCMT for two sources in $SiO(5 \rightarrow 4)$, the intensity in a 33″ beam is higher by 8% and 15% than in 46″ and 57″ beams, respectively. This is caused by the structure of the individual sources, and the numbers are, therefore, uncertain. We will, however, use these as correction factors when comparing HHT $SiO(5 \rightarrow 4)$ data to measurements obtained with larger beamsizes.

To adjust the calibration scales of the three telescopes, we have observed a number of sources in the 1.3 mm band which is accessible to all instruments (see Table 1). For $C^{18}O(2 \rightarrow 1)$, the integrated intensities at the 15 m-telescopes SEST and JCMT agree to better than 10%, i.e. to within the uncertainty of the calibration of the individual measurement. The $SiO(5 \rightarrow 4)$ JCMT maps, convolved to the larger size of the HHT beam, also give intensities that are consistent to within 10% with the HHT data. Thus, the $T_{\rm MB}$-scales are in excellent agreement, and we are confident that our complete data set has been placed on a compatible intensity scale.

We carried out all observations employing position switching. This was necessary given the large angular extent of the sources, especially in $C^{18}O$. Offset positions were typically chosen 15′ (SiO) or 30′ ($C^{18}O$) away from the source, perpendicular to the Galactic plane. This observing mode causes baselines that are not always perfectly flat. Thus, polynomial baselines of order ≤ 3 were subtracted from the data. Baselines were determined over a region of $\pm(150 - 200)\,{\rm km\,s^{-1}}$ from the line center. For the JCMT data, which were observed in exceptionally good weather ($\tau_{225} < 0.05$ throughout), linear baselines were usually sufficient.

For the final analysis, all spectra were smoothed to a velocity resolution of $\sim 2\,{\rm km\,s^{-1}}$.

3. Results

The 33 sources we study in detail are selected as distinct peaks in the CS survey of Bally et al. (1987). They are, therefore, cores that should have large amounts of dense gas, which are embedded in a smooth, lower intensity molecular intercloud medium. Since we wish to derive the properties of typical clouds in the Galactic center environment, the non-typical molecular peaks associated with Sgr A and Sgr B2 were not included in the sample.

The $(1 \rightarrow 0)$ and $(2 \rightarrow 1)$ transitions of $C^{18}O$ and the $(2 \rightarrow 1)$ transition of ^{28}SiO were observed toward all sources of our sample. Both the $C^{18}O$ and (more notably) the SiO lines were easily seen in all sources. We observed the 10 strongest $C^{18}O$ sources in the $(3 \rightarrow 2)$ submillimeter transition of $C^{18}O$, again detecting all. The rare isotopomers ^{29}SiO and ^{30}SiO were observed and detected toward 12 clouds showing strong emission in ^{28}SiO. Of 8 sources measured in the $^{28}SiO(5 \rightarrow 4)$ line, 7 showed emission. In Fig. 1 and Table 2, we give an overview of our results. Sample spectra for eight sources are displayed in Fig. 1. We mark the position of all sources observed on a survey map of the $(1 \rightarrow 0)$ transition of $C^{18}O$ (Papers I and II). Galactic coordinates are used for source names. For the cor-

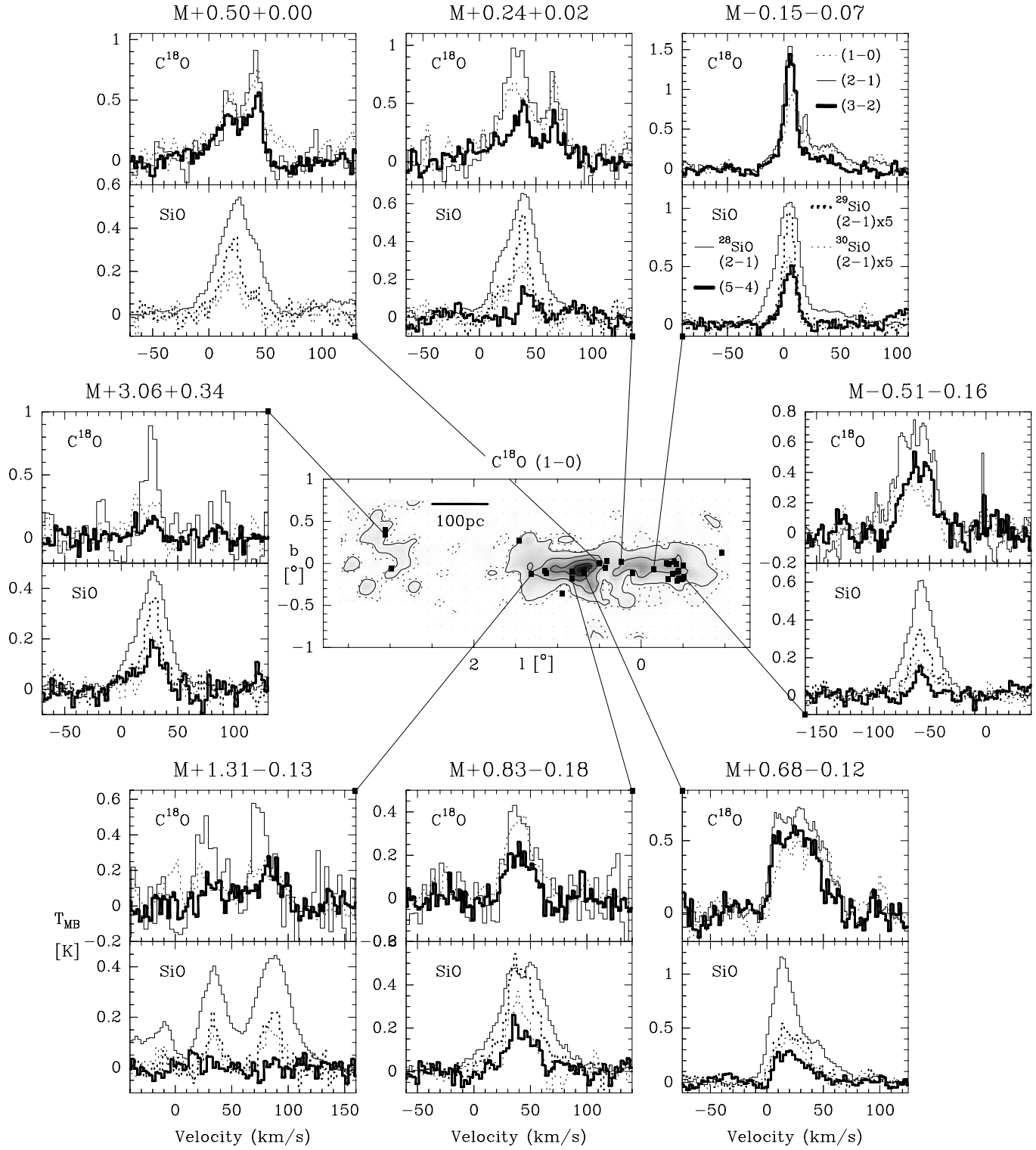

Fig. 1. Sample spectra of eight sources with very complete observations. In the top panels, the $C^{18}O$ lines are displayed: The $(1 \rightarrow 0)$ transition is drawn as a dotted line, the $(2 \rightarrow 1)$ transition is drawn as a thin solid line and the $(3 \rightarrow 2)$ transition is displayed as a thick solid line. The bottom panels show the SiO spectra. $^{28}SiO(2 \rightarrow 1)$ is denoted as a thin solid line, $^{28}SiO(5 \rightarrow 4)$ is given by a thick solid line; the $^{29}SiO(2 \rightarrow 1)$ spectrum is drawn as a thick dotted line and the $^{30}SiO(2 \rightarrow 1)$ is shown as a thin dotted line. The intensities of both rare isotopomers were multiplied by 5 to allow clearer comparisons. Black squares overlayed on the map of the overall distribution of the $J = 1 \rightarrow 0$ line of $C^{18}O$ (taken from Paper I) mark all 33 sources we observed except Clump 1 at $l \sim -5°$.

Table 1. Summary of the observations

Line	Frequency	Telescope	Receiver[a)]	$T_{\rm sys}$[b)]	$\theta_{\rm B}$	$\eta_{\rm MB}$	Spectrometer			Date
							Type[c)]	Bandwidth	Resolution	
	GHz			K	$''$			MHz	kHz	
$C^{18}O(1\rightarrow 0)$	109.782160	SEST	Schottky SSB	400	46	0.72	AOS	86	80	9/90,7/92
$C^{18}O(2\rightarrow 1)$	219.560319	SEST	SIS SSB	700–1100	24	0.55	AOS	995	1400	7&9/92
		JCMT[d)]	SIS DSB	600	20	0.69	DAS	250	189	4/96
$C^{18}O(3\rightarrow 2)$	329.350500	JCMT	SIS DSB	1600–1800	14	0.58	DAS	500	378	4/96
$^{28}SiO(2\rightarrow 1)$	86.846998	SEST	Schottky SSB	350–400	57	0.75	AOS	86	80	10/94
$^{28}SiO(5\rightarrow 4)$	217.104935	HHT	SIS DSB	700	33	0.83	AOS	990	1000	4/97
		JCMT[e)]	SIS DSB	600	20	0.69	DAS	250	189	4/96
$^{29}SiO(2\rightarrow 1)$	85.759132	SEST	SIS SSB	140	57	0.75	AOS	86/995	80/1400	3/96
$^{30}SiO(2\rightarrow 1)$	84.746036	SEST	SIS SSB	140	57	0.75	AOS	86/995	80/1400	3/96

a): SSB: Single sideband receiver, with a sideband rejection of ~ 20 dB ; DSB: Double sideband receiver
b): on a $T_{\rm MB}$ scale
c): AOS: Acousto-Optical Spectrometer; DAS: Dutch Autocorrelation Spectrometer
d): Only three sources were observed for cross-telescope calibration with SEST
e): Only two sources were observed for cross-telescope calibration with the HHT

responding equatorial coordinates, refer to Hüttemeister et al. (1993b). Most of the clouds we have studied are located within the molecular bulge region, while three lie within the 'Clump 2' complex (Bania 1977, Stark & Bania 1986) at $l\sim 3^\circ$. 'Clump 1' is located $\sim 5^\circ$ south of the Galactic center.

Integrated line intensities for the $C^{18}O(2\rightarrow 1)$ and $^{28}SiO(2\rightarrow 1)$ transitions and line intensity ratios derived from integrated intensities are presented in Table 2. The errors are determined from the (usually small) formal error of a Gaussian fit to the lines or, in case of non-Gaussian lineshapes, from the rms noise in the spectrum. In addition, a calibration uncertainty of 10% for data taken with the same telescope or 20% for data obtained with different instruments was assumed. For Gaussian lines, the formal error of the fit agrees closely with the error obtained from the rms noise in the spectrum.

For a given species, the center velocities and lineshapes of the different transitions always agree, to within the noise. Between SiO and $C^{18}O$, however, there can be significant differences. The sources M+0.50+0.00 and M+0.24+0.02 are good examples: In both cases, the $C^{18}O$ lines show two distinct peaks, while the SiO transitions are single-peaked. In M+0.50+0.00, the central velocity of the SiO is close to the weaker $C^{18}O$ line; in M+0.24+0.02 SiO and the stronger $C^{18}O$ peak agree. It is also noteworthy that narrow $C^{18}O$ lines close to a $v_{\rm LSR}$ of $0\,{\rm km\,s^{-1}}$, likely of local origin, never have a counterpart in SiO. This is illustrated by the source M–0.51–0.16 in Fig. 1 and demonstrates the unusual nature of the Galactic center sources as compared to Galactic disk clouds.

Since the lines of ^{29}SiO and ^{30}SiO are very likely optically thin, we can directly check whether the ratio of $^{29}Si/^{30}Si$ in the Galactic center region agrees with the terrestrial value. We find a line intensity ratio of 1.6 ± 0.2 in our sample, in excellent agreement with the terrestrial isotope ratio of 1.5. This confirms that this ratio does not depend on the galactocentric distance (Wilson & Rood 1994, Penzias 1981), which is an expected result if both isotopes are synthesized in the s-process in stars of the same type.

For $^{28}SiO/^{29}SiO$, we take the ratio to be the terrestrial value of 20, as suggested by Penzias (1981). Since the $^{28}SiO(2\rightarrow 1)$ transition is optically thick, we cannot check this assumption, but it is supported by the largest line ratio $r^{\rm SiO}_{28/29}$ (toward the exceptional source M+1.31–0.13, see Sect. 4.3), which is indeed close to 20.

4. The physical conditions of the gas

4.1. Determinination of densities and temperatures

A Large Velocity Gradient (hereafter LVG) model was used to estimate physical conditions of the gas, namely density ($n\,({\rm H_2})$), kinetic temperature ($T_{\rm kin}$) and – in the case of SiO – molecular abundance (X(SiO)) (see Scoville & Solomon 1974 and De Jong et al. 1975 for the general properties). We used a modified version of the code of Henkel et al. (1980). The basic LVG assumption is that a of systematic velocity gradient large compared to random motions and monotonic. This allows us to treat the molecular excitation as a local problem. This is certainly an idealisation for Galactic center clouds. However, an application of an LVG code requires no detailed knowledge of the velocity field. In the case of CO lines, H_2 densities determined under the assumption of LVG and microturbulence (the opposite extreme) do not differ by more than a factor of three (White 1977).

Our analysis is also based on the assumption that, for a given molecule, all transitions observed arise in the same volume. Since the excitation depends on critical density and optical depth, and thus is not identical for different transitions or different isotopomers, this assumption may not be strictly correct, especially if the medium is very clumpy (see, e.g., the discussion in Oka et al. 1998 for ^{12}CO). For $C^{18}O$, this is not a

Table 2. Integrated intensities of the $C^{18}O(2 \rightarrow 1)$ and $SiO(2 \rightarrow 1)$ transitions and line intensity ratios of $C^{18}O$ and SiO.

Source	$v_{\rm LSR}^{\rm C^{18}O}$	$I_{(2-1)}^{\rm C^{18}O}$	$\mathcal{R}_{2/1}^{\rm C^{18}O}$	$\mathcal{R}_{3/2}^{\rm C^{18}O}$ 10^{15}	$v_{\rm LSR}^{\rm SiO}$	$I_{(2-1)}^{\rm ^{28}SiO}$	$\mathcal{R}_{5/2}^{\rm ^{28}SiO}$	$r_{28/29}^{\rm SiO}$	$r_{29/30}^{\rm SiO}$ 10^{13}
	km/s	K km/s			km/s	K km/s			
Clump 1	97	4.5(0.2)	1.46(0.27)		97	0.6(0.2)			
M–0.96+0.13	135	5.1(0.5)	1.31(0.24)[a]		135	4.6(0.3)			
M–0.50–0.03	–100	15.3(0.4)	1.44(0.16)	0.49(0.11)	–98	4.0(0.3)			
	–2	1.6(0.2)	1.12(0.31)[c]	0.38(0.11)[c]	–2	≤ 0.1			
M–0.42–0.01	–84	10.5(0.4)	1.05(0.12)		–80	3.4(0.2)			
	–4	2.2(0.3)	1.35(0.34)		–4	≤ 0.2			
M–0.39+0.02	–80	13.8(1.2)	1.89(0.27)		–79	3.3(0.2)			
M–0.33–0.01	–47	12.8(0.5)	1.19(0.18)		–51	4.4(0.2)			
M–0.45–0.09	–61	4.0(0.4)	0.77(0.25)[a]		–61	≤ 0.3	–	–	
	–10	11.4(0.5)	2.09(0.39)		–12	16.7(1.5)	0.23(0.05)	15.9(3.1)	
M–0.30+0.00	–33	12.1(0.7)	1.23(0.25)[b]		–38	5.0(0.3)			
M–0.44–0.10	–15	6.1(0.6)	0.60(0.31)[a),b]		–20	19.8(2.0)		12.3(1.8)	1.7(0.3)
M–0.51–0.16	–61	27.2(0.8)	2.67(0.14)	0.51(0.08)	–57	30.6(0.5)	0.09(0.03)	11.0(1.4)	1.6(0.3)
	–2	1.7(0.2)	1.33(0.75)[c]	0.41(0.14)[c]	–2	≤ 0.1	–	–	–
M–0.50–0.18	–57	14.3(0.7)	2.40(0.67)		–55	9.3(0.4)			
M–0.48–0.19	–50	6.9(0.4)	1.47(0.32)[a]		–53	4.0(0.2)			
M–0.38–0.13	–33	10.4(0.7)	1.11(0.26)	0.57(0.12)	–32	1.7(0.2)			
M–0.45–0.19	21	4.5(0.2)	1.10(0.19)[c]		21	≤ 0.2			
	58	3.9(0.3)	0.50(0.31)[a]		58	5.8(0.2)			
M–0.43–0.21	–34	22.4(0.9)	2.07(0.27)		–27	6.5(0.3)			
	19	3.5(0.3)	1.13(0.21)[c]		19	≤ 0.2			
	53	2.7(0.6)	0.71(0.22)[a]		54	5.7(0.4)			
M–0.15–0.07	5	37.5 (0.4)	1.40(0.15)[b]	0.75(0.14)[b]	4	31.5(1.1)	0.19(0.04)[b]	11.3(1.3)	1.6(0.2)
M–0.32–0.19	–32	7.3(0.7)	1.22(0.28)[a]						
	25	$\leq$3.0			25	2.9(0.2)			
M+0.24+0.02	35	41.7(3.7)	1.06(0.16)[b]	0.51(0.11)[b]	36	24.4(0.7)	0.07(0.02)	11.4(1.3)	1.6(0.3)
M+0.10–0.12	22	22.1(0.9)	1.46(0.21)		29	11.5(1.2)			
M+0.43–0.05	–2	4.5(0.3)	0.95(0.28)[a]		12	11.0(0.8)		13.3(2.2)	
	38	4.9(0.3)	0.69(0.15)[a]						
M+0.41+0.03	30	10.5(0.4)	0.64(0.10)[b]		21	10.4(1.1)			
M+0.50+0.00	30	22.9(2.4)	1.06(0.21)[b]	0.76(0.15)[b]	26	20.9(0.3)		13.1(2.1)	1.7(0.3)
M+0.68–0.12	30	35.4(0.3)	1.48(0.17)[b]	0.70(0.14)[b]	20	39.2(2.3)	0.18(0.05)[b]	11.9(1.4)	1.2(0.2)
M+0.83–0.10	24	13.4(0.8)	0.81(0.18)[a),b]		24	10.4(0.4)			
	99	8.7(0.5)	1.66(0.29)		96	2.5(0.2)			
M+1.46+0.27	80	6.6(0.4)	0.95(0.32)[a]		81	20.4(0.3)		13.8(1.6))[b]	1.5(0.3)
M+0.83–0.18	41	10.6(1.0)	1.03(0.13)	0.53(0.12)	43	26.0(0.4)	0.19(0.04)	7.4(0.8)	2.0(0.2)
M+1.15–0.09	–18	1.9(0.2)	1.05(0.20)[c]		–18	≤ 0.2			
	60	7.8(1.2)	0.68(0.23)[a),b]		67	21.0(1.1)			
M+1.13–0.12	–15	12.9(0.9)	1.48(0.18)		–15	6.4(0.7)			
	80	1.8(0.3)	0.47(0.22)[a]		70	17.5(1.2)			
M+1.31–0.13	30	11.6(0.6)	1.95(0.39)[a]	0.25(0.13)[a]	35	11.5(0.5)	≤ 0.04[d]	20.9(2.3)	1.5(0.3)
	80	7.8(0.6)	1.58(0.35)[a]	0.78(0.26)[a]	87	16.8(0.5)	≤ 0.04[d]	18.0(2.7)	1.4(0.2)
M+0.94–0.36	–49	18.5(1.3)	2.05(0.33)[b]		–41	3.4(0.5)			
M+3.06+0.40	12	1.6(0.1)	0.82(0.15)[c]		12	≤ 0.1			
	22	2.5(0.3)	0.61(0.16)[a]		30	9.3(2.1)			
M+3.06+0.34	27	12.1(3.6)	1.49(0.48)	0.24(0.09)	27	15.2(0.3)	0.16(0.06)	10.1(1.2)	1.9(0.4)
M+2.99-0.06	–13	2.6(0.3)	1.21(0.27)		–12	8.5(0.3)			

Abbreviations used throughout the paper: $\mathcal{R}_{2/1}^{\rm C^{18}O} = I_{(2-1)}^{\rm C^{18}O}/I_{(1-0)}^{\rm C^{18}O}$, $\mathcal{R}_{3/2}^{\rm C^{18}O} = I_{(3-2)}^{\rm C^{18}O}/I_{(2-1)}^{\rm C^{18}O}$, $\mathcal{R}_{5/2}^{\rm ^{28}SiO} = I_{(5-4)}^{\rm ^{28}SiO}/I_{(2-1)}^{\rm ^{28}SiO}$, $r_{28/29}^{\rm SiO} = I_{(2-1)}^{\rm ^{28}SiO}/I_{(2-1)}^{\rm ^{29}SiO}$, $r_{29/30}^{\rm SiO} = I_{(2-1)}^{\rm ^{29}SiO}/I_{(2-1)}^{\rm ^{30}SiO}$

a): The result is uncertain, due to either baseline uncertainties or low signal-to-noise ratios

b): Non-gaussian lineshape or several blended velocity components; ratios have been calculated by adding channels with emission

c): very narrow line, possibly from local ISM

d): 3σ

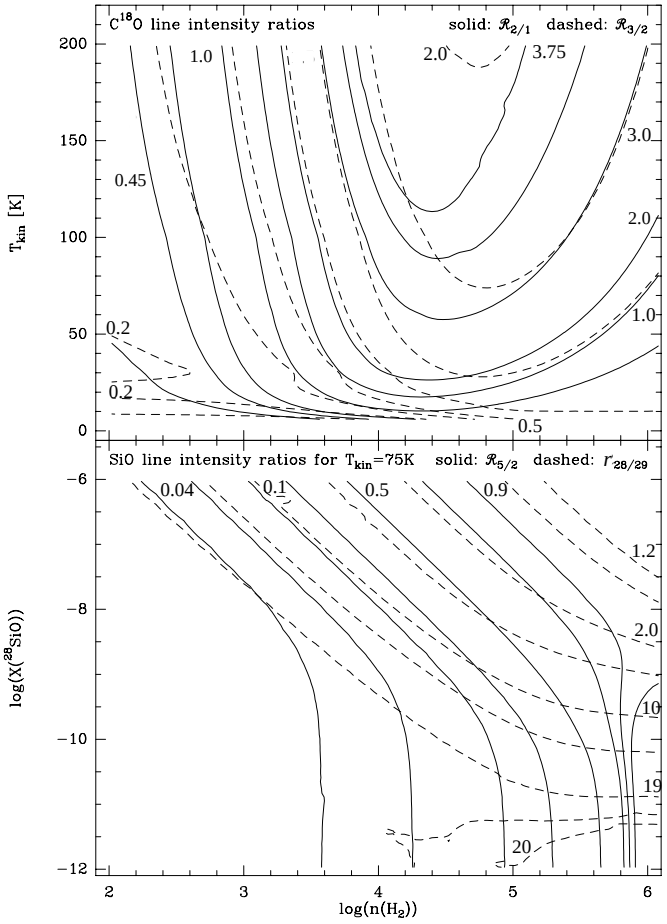

Fig. 2. Line intensity ratios from our LVG model calculations for $C^{18}O$ (upper panel) and ^{28}SiO and ^{29}SiO (lower panel). The contours are at:
$\mathcal{R}^{C^{18}O}_{2/1}$(solid): 0.3, 0.45, 0.6, 1.0, 1.5, 2.0, 3.0, 3.5, 3.75
$\mathcal{R}^{C^{18}O}_{3/2}$(dashed): 0.1, 0.2, 0.35, 0.5, 0.75, 1.0, 1.5, 2.0
$\mathcal{R}^{^{28}SiO}_{5/2}$(solid): 0.04, 0.05, 0.1, 0.2, 0.5, 0.8, 0.9, 1.0
$r^{SiO}_{28/29}$(dashed): 1.2, 1.5, 2.0, 5.0, 10.0, 15.0, 19.0, 19.75, 20.0

critical problem since the LVG calculations show that all transitions measured by us are optically thin, or, in the low temperature/high density scenario described below, reach, at most, $\tau \approx 1$. Therefore, $C^{18}O$ line intensity ratios are not strongly affected by the possibly different locations of cloud 'photospheres' from which the bulk of the photons are emitted. All transitions of $C^{18}O$ should trace all molecular gas at densities $\geq 10^3$ cm^{-3}, as long as $C^{18}O$ is not selectively dissociated by UV radiation. Away from the star forming regions Sgr A and Sgr B2, the UV radiation field in the Galactic center region is not likely to be strong (e.g. Nagakawa et al. 1995). In addition, because we are considering density peaks of the molecular gas (and dust), the destruction of $C^{18}O$ should not be a problem; from the H_2 column densities derived below, dust extinction is likely to provide sufficient shielding.

In our model calculations, the population $n(J)$, excitation temperature $T_{\rm ex}$, brightness temperature $T_{\rm B}$, and optical depth τ, are determined for each rotational level up to a maximum $J = 20$ for $C^{18}O$ and $J = 13$ for SiO. Collision rates are taken from Green & Chapman (1978). We have chosen a constant velocity gradient of $5\,{\rm km\,s^{-1}\,pc^{-1}}$, a value estimated from the velocity extent and diameter of Galactic center clouds as mapped by Bally et al. (1987) or Lindquist et al. (1995). The background continuum temperature was assumed to be 2.7 K.

4.1.1. $C^{18}O$

We assume that the abundance of $C^{18}O$ relative to H_2 is $4\cdot10^{-7}$. This ratio is based on the standard Galactic center $^{16}O/^{18}O$ isotopic ratio of 250 (Wilson & Matteucci 1992, Wilson & Rood 1994) and a CO/H_2 ratio of 10^{-4} (e.g. Frerking et al. 1982, Duvert et al. 1986 (dark clouds), Blake et al. 1987 (OMC-1)). According to the calculations of Farquhar et al. (1994), this ratio is stable against a possibly enhanced cosmic ray flux close to the Galactic center. For $C^{18}O$, we then calculate a grid by varying the H_2 density, $n\,(H_2)$, from 10^2 cm^{-3} to 10^6 cm^{-3} and the kinetic temperature, $T_{\rm kin}$, from 5 to 200 K.

We found the range of $n\,(H_2)$ and $T_{\rm kin}$ by comparing the observed line intensity ratios (Table 2) to the ratios predicted by the model (Fig. 2). It is important to use line intensity ratios, not just intensities, since intensities are affected by an a priori unknown beam filling factor, $f_{\rm b}$. For the intensity ratios, we took $f_{\rm b}$ to be identical for all transitions of a given molecule.

The integrated intensity ratio of the $C^{18}O(2 \rightarrow 1)$ to $(1 \rightarrow 0)$ transition, $\mathcal{R}^{C^{18}O}_{2/1}$, from all sources is 1.3 ± 0.5, with extreme values ranging from 0.5 to ~ 2. The ratio of the $(3 \rightarrow 2)$ to the $(2 \rightarrow 1)$ intensity, $\mathcal{R}^{C^{18}O}_{3/2}$, is 0.5 ± 0.2. Averaged over all sources, the LVG model fits yield $T_{\rm ex} = 11(\pm4)$ K for the $C^{18}O(2 \rightarrow 1)$ transition, that is, $C^{18}O$ is subthermally excited. The beam averaged peak optical depth τ_{21} is always < 0.2. The measured peak temperatures $T_{\rm MB}$ indicate a beam filling factor $f_{\rm b}^{C^{18}O}$ of ~ 1 for $n\,(H_2) = (2-4)\,10^3$ cm^{-3}. $f_{\rm b}^{C^{18}O}$ is lower if $n\,(H_2)$ is higher. From the structure seen in our maps of the $C^{18}O(1\rightarrow0)$ beam in higher transitions, we estimate $f_{\rm b}^{C^{18}O}$, averaged over all gas components, to be ~ 0.5. These maps, however, have a low signal-to-noise ratio.

From the model calculations (Fig. 2, upper panel), maximum values up to 4 in $\mathcal{R}^{C^{18}O}_{2/1}$ and up to 2 in $\mathcal{R}^{C^{18}O}_{3/2}$ are expected for hot ($T_{\rm kin} > 100$ K) and dense ($n\,(H_2) \sim 10^4 - 10^5$ cm^{-3}) gas. Such high ratios are reached in none of our sources. Possible combinations of $n\,(H_2)$ and $T_{\rm kin}$ are *either* a high $T_{\rm kin}$ of ≥ 100 K and $n\,(H_2)$ of $(1-4)\,10^3$ cm^{-3} *or* a lower $T_{\rm kin}$ (≤ 20 K – 30 K) at a higher $n\,(H_2) \geq 10^4$ cm^{-3}. We have carried out this analysis individually for all clouds. For all sources our $C^{18}O$ data *unambiguously* require gas with densities of $\geq 10^4$ cm^{-3} in these Galactic center clouds to be *cool*.

From ammonia measurements (Hüttemeister et al. 1993b) it is known that both hot and cool gas is present within the area covered by our beam. Thus, it is likely that both scenarios possible from the $C^{18}O$ data are realized. A continuum of temperatures and densities is compatible with our data. Then $T_{\rm kin}$ rises steadily as $n\,(H_2)$ decreases, when the line of sight samples different parts of the cloud. Density peaks (indicated by strong

CS lines) in Galactic center region GMCs not presently undergoing massive star formation can be regarded as *'cool dense cores'* in contrast to the hot dense cores generally encountered within GMCs in the disk.

4.1.2. SiO

It has been shown that the fractional abundance of SiO, X(SiO), can change by more than six orders of magnitude between quiescent cold material and hot, shocked dense gas (Ziurys et al. 1989, Martín-Pintado et al. 1992). Since SiO is readily detected in all our sources, X(SiO) *cannot* be low. However, we cannot assume any specific value. Therefore, we have used X(SiO) as a free parameter in the models, varying it from 10^{-12} to 10^{-6}. Grids have been calculated as a function of $n\,(\mathrm{H_2})$ and X(SiO) for $T_{\rm kin}$= 25 K, 50 K, 75 K, 100 K, 150 K.

The average line intensity ratio between the SiO $(5 \rightarrow 4)$ and $(2 \rightarrow 1)$ transition is $\mathcal{R}_{5/2}^{^{28}\mathrm{SiO}} = 0.16 \pm 0.05$, for those sources where we detected SiO$(5 \rightarrow 4)$. M+1.31–0.13 is exceptional and will be discussed further in Sect. 4.3. Since the signal-to-noise (S/N) ratio in the $(5 \rightarrow 4)$ line is not always high and the $(2 \rightarrow 1)$ SEST beam was not mapped in this transition, it is not clear whether source to source differences (apart from M+1.31–013) are significant. For the line ratios between the $(2 \rightarrow 1)$ transitions of ^{28}SiO and ^{29}SiO (excluding M+1.31–0.13), we find a mean ratio of $r_{28/29}^{\mathrm{SiO}} = 12.2 \pm 2.2$ with extreme values ranging from 7.4 to 15.9. Since these data, even in the ^{29}SiO transition, have very good S/N ratios and were measured with the same telescope and beamsize, there is no doubt that the source-to-source differences are significant.

Fig. 2 (lower panel) shows the line ratios $\mathcal{R}_{5/2}^{^{28}\mathrm{SiO}}$ and $r_{28/29}^{\mathrm{SiO}}$ for $T_{\rm kin}$= 75 K from our LVG calculations. Lowering $T_{\rm kin}$ to 25 K requires a slight increase of the $\mathrm{H_2}$ densities for a given line ratio, by a factor of ~ 1.25. Raising $T_{\rm kin}$ to 150 K corresponds to slightly lower densities. In general, the effects of changing $T_{\rm kin}$ on the line ratios are negligible: SiO line ratios are almost insensitive to cloud temperature.

To derive $T_{\rm ex}$ and $n\,(\mathrm{H_2})$, we have analysed all sources individually. Excluding M+1.31–0.13, we find $T_{\rm ex}$ ranging from 5 K to 10 K. $n\,(\mathrm{H_2})$ changes with the assumed SiO abundance: A higher X(SiO) requires a lower $\mathrm{H_2}$ density (Fig. 2). Curves of constant $\mathcal{R}_{5/2}^{^{28}\mathrm{SiO}}$ and $r_{28/29}^{\mathrm{SiO}}$ run parallel for a range of densities and SiO abundances. Typical ranges are $X(\mathrm{SiO}) \approx 10^{-6}$ for $n\,(\mathrm{H_2}) \approx (1 - 2.5)\,10^3$ cm^{-3} to $X(\mathrm{SiO}) \approx 10^{-9}$ for $n\,(\mathrm{H_2}) \approx 4\,10^4 - 10^5$ cm^{-3}. Lower SiO abundances or higher densities are not possible, since then the curves diverge.

Plotting the measured $T_{\rm MB}$'s for the ^{28}SiO$(2 \rightarrow 1)$ transition in the LVG plots (e.g. Fig. 3, lower left panel), we find that a considerably higher $T_{\rm B}$ is needed to fit the observed line ratios. Thus we estimate that the beam filling factor $f_{\rm b}^{\rm SiO}$ ($T_{\rm MB} = f_{\rm b}^{\rm SiO}\,T_{\rm B}$) is ~ 0.2 for the 'typical' sources.

This analysis is biased toward more intense SiO lines, since only those were observed in transitions other than ^{28}SiO$(2 \rightarrow 1)$. The strength in SiO toward these positions may be either due to a large amount of molecular gas, or to an abundance of SiO that is above average. This question will be addressed in the next section.

4.2. A joint view of $C^{18}O$ and SiO

4.2.1. Column densities and SiO abundances

Further insight in the structure of the clouds is gained by combining what can be learned from $\mathrm{C^{18}O}$ and SiO.

We calculate the total (beam averaged) column densities for $\mathrm{C^{18}O}$ and ^{28}SiO, applying the same procedure to both molecules: First, we use the observed $T_{\rm MB}$ and the best fit $T_{\rm ex}$ from the LVG model for the $(2 \rightarrow 1)$ transitions (the lines with the best S/N ratio) to calculate the (beam averaged) optical depth $\bar{\tau}_0$. Taking $\int \bar{\tau}(v)\,\mathrm{d}v = 1.06\,\bar{\tau}_0\,\Delta v_{1/2}$, we then derive the column density in the $J = 1$ level, $\bar{N}_1$. The total beam averaged column density $\bar{N}$ is determined by dividing $\bar{N}_1$ by the fraction of the population residing in the $J = 1$ level, derived from the LVG model. (See Rohlfs & Wilson (1996) for a collection of the (standard) formulae we used.) For non-gaussian lines, the second moment of the line has been used as a measure of the line width instead of $\Delta v_{1/2}$. This has been combined with a $T_{\rm MB}$ which reproduces the observed integrated intensity. This is correct as long as $T_{\rm ex}$ does not change across the line profile. Since the line shapes in all transitions observed for a given molecule agree closely, this is a reasonable assumption.

For the sources where we observed only the SiO$(2 \rightarrow 1)$ line, we have used average values for $T_{\rm ex}$ and the fraction of the population in the $J = 1$ level. These are 7 K and 0.36, respectively. Total beam averaged column densities are given in Table 3.

The usually optically thin, easily excited transitions of $\mathrm{C^{18}O}$ are known to be excellent tracers of $\mathrm{H_2}$ column density, $\bar{N}_{\mathrm{H_2}}$, over a wide variety of $\mathrm{H_2}$ densities and kinetic temperatures. In particular, the integrated intensity of the $J = 2 \rightarrow 1$ transition can be directly related to $\bar{N}_{\mathrm{H_2}}$ (Genzel 1992). Our LVG modelling confirms that for a large range of temperatures the fraction of the total population in the $\mathrm{C^{18}O}$ $J = 1$ level remains almost constant between $n\,(\mathrm{H_2}) = 10^2$ cm^{-3} and 10^4 cm^{-3}.

In most cases, we find that column densities agree with the formula given by Mauersberger et al. (1992) and Genzel (1992) ($\bar{N}_{\mathrm{H_2}} = 1.12\ 10^{21} \int T_{\rm MB}^{\mathrm{C^{18}O}}(2 \rightarrow 1)\,\mathrm{d}v$ for the Galactic center isotopic ratios) to within 10%. Differences up to a factor of 2 are found if the excitation temperature is exceptionally low.

The knowledge of $\bar{N}_{\mathrm{H_2}}$ and $\bar{N}^{\rm SiO}$ allows us to derive a beam averaged SiO relative abundance, assuming that the $\mathrm{C^{18}O}$ and SiO emission arises from the same gas. This is given in Table 3, and typically ranges from $0.5\,10^{-9}$ to $5\,10^{-9}$. Since $\mathrm{C^{18}O}$ presumably traces *all* $\mathrm{H_2}$ with $n\,(\mathrm{H_2}) \geq 10^3$ cm^{-3}, the true abundance of SiO cannot be *lower* than the value thus determined. It can be higher, if only part of the gas within the beam is abundant in SiO, which, considering the differences in line centers and line profiles between $\mathrm{C^{18}O}$ and SiO (e.g. M+0.24+0.02, see Fig. 1), is likely.

For those sources where the SiO$(2 \rightarrow 1)$ transition is weak and which were only observed in this SiO transition, the $\mathrm{H_2}$

Table 3. Total beam averaged column densities of $C^{18}O$ ($\bar{N}^{C^{18}O}$) and SiO ($\bar{N}^{SiO}$) and beam averaged abundances of SiO, X(SiO). $\bar{N}^{H_2}$ follows from $\bar{N}^{C^{18}O}$, assuming $X(C^{18}O)$ to be $4 \cdot 10^{-7}$. Errors are given in parentheses.

Source	$v_{LSR}^{C^{18}O}$	$\bar{N}^{C^{18}O}$	v_{LSR}^{SiO}	$\bar{N}^{SiO}$	X^{SiO}
		10^{15}		10^{13}	10^{-9}
	km/s	cm^{-2}	km/s	cm^{-2}	
Clump 1	97	2.6(0.9)	97	~ 0.1	0.1
M–0.96+0.13	135	2.9(1.1)	135	~ 0.9	1.7
M–0.50–0.03	–100	8.9(1.4)	–98	~ 0.8	0.4
	–2	1.1(0.2)	–2	< 0.02	< 0.07
M–0.42–0.01	–84	7.5(0.8)	–80	~ 0.6	0.3
	–4	1.2(0.1)	–4	< 0.1	< 0.03
M–0.39+0.02	–80	6.6(0.6)	–79	~ 0.6	0.4
M–0.33–0.01	–47	7.7(2.5)	–51	~ 0.8	0.4
M–0.45–0.09	–61	3.6(0.9)	–61	< 0.09	< 0.1
	–10	5.5(0.5)	–12	3.2(0.4)	2.3
M–0.30+0.00	–33	7.2(1.5)	–38	~ 1.0	0.6
M–0.44–0.10	–15	7.4(2.9)	–20	4.4(1.0)	2.4
M–0.51–0.16	–61	13.1(3.5)	–57	4.0(1.5)	1.2
	–2	1.0(0.3)	–2	< 0.03	< 0.1
M–0.50–0.18	–57	7.6(1.5)	–55	~ 1.8	1.0
M–0.48–0.19	–50	3.6(0.8)	–53	~ 0.7	0.7
M–0.38–0.13	–33	6.6(0.9)	–32	~ 0.3	0.2
M–0.45–0.19	21	3.0(0.5)	21	< 0.04	< 0.05
	58	4.4(1.0)	58	~ 1.1	1.0
M–0.43–0.21	–34	10.4(0.4)	–27	~ 1.2	0.5
	19	2.2(0.3)	19	< 0.04	< 0.07
	53	2.8(0.6)	54	~ 1.1	0.6
M–0.15–0.07	5	19.1(1.0)	4	6.2(1.0)	1.3
M–0.32–0.19	–32	4.3(0.7)			
	25	≤ 1.6	25	~ 0.6	> 1.5
M+0.24+0.02	35	26.1(5.0)	36	5.6(1.2)	0.9
M+0.10–0.12	22	11.5(1.9)	29	~ 2.2	0.8
M+0.43–0.05	–2	3.4(0.8)	12	2.4(0.6)	2.8
	38	4.9(0.9)			
M+0.41+0.03	30	14.1(1.0)	21	~ 2.0	0.6
M+0.50+0.00	30	13.2(2.9)	26	5.0(1.6)	1.5
M+0.68–0.12	30	17.2(2.0)	20	7.6(0.7)	1.8
M+0.83–0.10	24	12.1(3.5)	24	~ 1.9	0.6
	99	4.4(0.4)	96	~ 0.5	0.5
M+1.46+0.27	80	4.9(1.3)	81	4.9(1.0)	4.0
M+0.83–0.18	41	6.8(1.6)	43	4.9(0.2)	2.9
M+1.15–0.09	–18	1.2(0.2)	–18	< 0.06	< 0.02
	60	8.9(1.9)	67	~ 4.0	1.8
M+1.13–0.12	–15	7.4(0.8)	–15	~ 0.5	0.3
	80	3.3(1.3)	70	~ 3.3	4.0
M+1.31–0.13	30	6.9(3.5)	35	~ 10	5.8
	80	4.0(0.4)	87	~ 10	10.0
M+0.94–0.36	–49	8.8(0.3)	–41	~ 0.6	0.3
M+3.06+0.40	12	1.5(0.3)	12	< 0.02	< 0.05
	22	3.7(1.0)	30	~ 1.7	1.8
M+3.06+0.34	27	10.0(3.0)	27	2.9(0.3)	1.2
M+2.99-0.06	–13	3.3(0.7)	–12	~ 1.6	1.9

column density obtained from $C^{18}O$ is not systematically lower than for the more intense sources. On average, in these clouds X(SiO) is lower by a factor of ~ 3. Source-to-source variations are significant, even though the properties in dense gas as traced by CS (Hüttemeister 1993) and total gas as traced by $C^{18}O$ do not differ. This agrees with the variation found in the survey of Martín-Pintado et al. (1997). Note, however, that we find SiO with an abundance that is high when compared to typical disk GMCs in all sources.

4.2.2. Density and temperature

We now combine the LVG models for $C^{18}O$ and SiO to derive a consistent solution for $n\,(H_2)$ and T_{kin}. This is done in terms of a two component model, where part of each $C^{18}O$ emission line is ascribed to a cool component, with the remaining part arising from a hot component.

From the NH_3 studies of Hüttemeister et al. (1993b), we know that, for a typical cloud, roughly 25% of the neutral gas mass is contained in the hot (> 100 K) component, which, from our $C^{18}O$ analysis, must have a low density. Thus, the remaining $\sim$ 75% of the total gas mass is at a density of $\geq 10^4\,cm^{-3}$. The hot, thin and the cool, dense component are roughly in pressure equilibrium. Let us assume that the SiO emission arises in only the cool, dense component. The corresponding relative abundances of SiO, X(SiO), are 25% above the beam averaged values given in Table 3. X(SiO) lies within the range allowed by the SiO line ratios (Fig. 2) and is consistent with an H_2 density of typically $(1-4)\,10^4\,cm^{-3}$. The beam filling factor f_b in this dense component must be the same for both the SiO and the part of the $C^{18}O$ emission that arises in this component.

We can estimate the main beam brightness temperature of the dense, $C^{18}O$ emitting gas to be 0.75 of the total $C^{18}O$ intensity. Using the beam filling factor determined for the dense gas from SiO lines, the brightness temperature of the $C^{18}O(2 \rightarrow 1)$ line is $T_B^{C^{18}O}(75\%) \approx 0.75\,T_{MB}\,/f_b$. This simple relation can be used since the $C^{18}O(2 \rightarrow 1)$ line has an optical depth ≤ 1. If the solution is self-consistent, the H_2 density indicated by this value of T_B and the observed line ratios must agree with the density derived for SiO. To within a factor of 2, we find that this is indeed the case. Thus, it is possible that the SiO emission originates in gas having $n\,(H_2) \sim (1-4)10^4\,cm^{-3}$. This gas must be relatively cool, which is a surprising result in the light of the clear association of the SiO emission with hot shocked gas in the Galactic disk. The intrinsic optical depth τ_0 of the $SiO(2 \rightarrow 1)$ then ranges from 4 – 8.

Can the SiO emission be associated with the hot, thin gas component? To check this, we used the same procedure as before: From the assumption that the SiO emission arises in $\sim 25\%$ of the gas, we get a value for X(SiO) and a corresponding H_2 density. The beam filling factor f_b for SiO and, consequently, for the part of $C^{18}O$ originating in the same gas does not change. Now, $T_B^{C^{18}O}(25\%) \approx 0.25\,T_{MB}\,f_b$. The additional requirement that this gas should be hot yields a H_2 density that is, for many clouds, lower by an order of magnitude than what is derived for the same component from SiO. Thus, this is not a consistent solution. If the SiO arises in a still smaller portion of the total gas, the discrepancy becomes even worse. Note that we do not

claim that the hot, thin component is devoid of SiO. We consider it likely that the SiO abundance in this component is similar to what we determine for the dense component. However, the SiO excitation in this component is extremely subthermal, leading (1) to lower line intensities than those we observe (specifically, no emission from the (5→4) transition) and (2) to different line intensity ratios.

Finally, we can rule out the presence of a hot, high density ($n\,(\mathrm{H_2}) \geq 10^4\,\mathrm{cm^{-3}}$) component as the origin of the SiO emission: We know from the line ratios $\mathcal{R}_{5/2}^{^{28}\mathrm{SiO}}$ and $r_{28/29}^{\mathrm{SiO}}$ that X(SiO) must decrease with increasing density, independent of T_{kin}. Thus, a hot, high density component containing the bulk of the SiO would have to contain a significant fraction of the total H_2 column density and mass. Such a component should be visible in $\mathrm{C^{18}O}$. Thus we conclude that it does not exist in these clouds.

Therefore the only consistent scenario that accounts for both the SiO and $\mathrm{C^{18}O}$ results requires that most of the SiO emission arises from a *cool* (20 K – 30 K) gas component with $n\,(\mathrm{H_2}) \sim 10^4\,\mathrm{cm^{-3}}$.

So far, we have *assumed that the* $\mathrm{C^{18}O}$ *abundance in all components considered is known and constant.* If this is not the case, i.e. if $\mathrm{C^{18}O}$ is *not* a reliable H_2 column density tracer, the line of argumentation given above cannot be maintained. In this case, it becomes possible to claim that the SiO emission arises in a hot, dense component not seen in $\mathrm{C^{18}O}$. This is, however, only possible if $\mathrm{C^{18}O}$ is selectively underabundant in the component where the SiO abundance is high. Since selective $\mathrm{C^{18}O}$ dissociation due to lack of shielding is efficient only in diffuse, low density gas (if the UV field is strong enough), it is difficult to find a scenario causing $\mathrm{C^{18}O}$ to be underabundant in dense, warm gas.

4.3. A detailed investigation of two sources

M+0.83–0.18 In Fig. 3 (left panels), we illustrate the procedure of deriving the physical cloud parameters described above for the source M+0.83–0.18. This is representative of the type of cloud where SiO emission arises in a cool, moderately dense component. The SiO line ratios in this source (lower left panel in Fig. 3) are well fit by $T_{\mathrm{ex}} = 10\,\mathrm{K}$. Then, X(SiO) is $3.9\,10^{-9}$ if SiO arises from 75% of the total gas. The observed T_{MB} is 0.48 K, while a T_{B} of 7.5 K is required to fit the range of $n\,(\mathrm{H_2})$ and X(SiO). This results in the lowest value for f_{b} of all sources, 0.06, and the highest optical depth τ_0, 8. Applying the same f_{b} to the $\mathrm{C^{18}O}$ data (upper left panel), we have $T_{\mathrm{B}}(\mathrm{C^{18}O}) = 0.75\,T_{\mathrm{MB}}/0.06 = 5.1\,\mathrm{K}$. If we take the resulting $n\,(\mathrm{H_2})$ from the SiO analysis, $4\,10^4\,\mathrm{cm^{-3}}$, and transfer this to $\mathrm{C^{18}O}$, we find that T_{kin} is only $\sim 12\,\mathrm{K}$. If we require T_{kin} to be identical to the value we have measured for the cool component from NH_3, 21 K (Hüttemeister et al. 1993b), the density obtained for $\mathrm{C^{18}O}$ is $2\,10^4\,\mathrm{cm^{-3}}$. Considering all the assumptions, there is satisfactory agreement. Could the results be consistent with the 'high temperature scenario' described in the last section? We find that $n\,(\mathrm{H_2})$ required from an analysis of the SiO data is $\sim 3\,10^4\,\mathrm{cm^{-3}}$, while the $\mathrm{C^{18}O}$ data at the appropriate T_{B} yield $\sim 3\,10^3\,\mathrm{cm^{-3}}$, clearly a far less consistent solution.

M+1.31–0.13 Now we analyze the one source which is very different from all the others in our sample: M+1.31–0.13 (right panels of Fig. 3). This is the only source where the $(5 \rightarrow 4)$ transition of ^{28}SiO was not detected, even though the $(2 \rightarrow 1)$ line is strong. It also is the one source where $r_{28/29}^{\mathrm{SiO}}$ approaches the terrestrial isotopic ratio of 20, indicating that τ_0 for ^{28}SiO$(2 \rightarrow 1)$ cannot be large. M+1.31–0.13 has two velocity components. We analyze the (slightly) more intense $v_{\mathrm{LSR}} \sim 85\,\mathrm{km\,s^{-1}}$ component, but the $v_{\mathrm{LSR}} \sim 35\,\mathrm{km\,s^{-1}}$ component shows the same characteristics.

From the SiO line ratios, we derive an extremely low excitation temperature, 3.2 K. The large column density for SiO depends strongly on the exact value of T_{ex}. Therefore, we can give only an estimate of $\bar{N}^{\mathrm{SiO}}$ in Table 3. The corresponding X(SiO) is $\sim 10^{-8}$, by far the highest in the sample. In addition, for this source we find $T_{\mathrm{MB}} = T_{\mathrm{B}}$, i.e. $f_{\mathrm{b}} = 1$. As expected, this results in a lower τ_0, ~ 2, in the ^{28}SiO$(2 \rightarrow 1)$ line. For the H_2 density, we find $n\,(\mathrm{H_2}) \approx 2\,10^3\,\mathrm{cm^{-3}}$. This is a factor of ~ 10 lower than for all other sources.

Since our calculations give $\tau_0 \sim 2$ and $f_{\mathrm{b}} = 1$ for SiO, we conclude that in this source SiO traces *all* the gas, as does $\mathrm{C^{18}O}$. Hence, $f_{\mathrm{b}} = 1$ and $T_{\mathrm{B}} = T_{\mathrm{MB}}$ is also valid for $\mathrm{C^{18}O}$. The resulting $n\,(\mathrm{H_2})$ from $\mathrm{C^{18}O}$ is $2\,10^3\,\mathrm{cm^{-3}}$, identical to the result obtained from SiO. As expected, T_{kin} is high, $> 100\,\mathrm{K}$. Thus, for this one source, we have found a fully self-consistent solution of an entirely different type: The SiO arises in thin, hot gas and has an abundance that is far above average, even for the clouds that are rich in SiO.

Is there evidence that M+1.31–0.13 lacks the dense and cool gas component? Remarkably, our NH_3 data show that this cloud is *the only one in the entire sample* in which the $(J, K) = (4, 4)$ inversion transition at 200 K above ground is more intense than the (1,1) transition at 23 K above ground. Thus, in this cloud a cool, dense gas component containing the bulk of the gas is not present. Most, perhaps all of the gas is hot and thin. Relating this to the high SiO abundance, it is likely that SiO does indeed form at high temperatures in the Galactic center region. In M+1.31–0.13, the SiO formation process is either still ongoing or has occured very recently. The SiO has not yet had time to recondense onto dust grains, and the cloud itself has not had time to form dense cool cores.

5. Discussion

5.1. Cloud properties as a tracer of large scale dynamics

We will now explore how the relative SiO abundances may be related to the position of the cloud in the large scale Galactic center environment.

In Fig. 4 we plot the the beam averaged SiO abundance, X^{SiO}, on a longitude-velocity diagram of the large scale distribution of $\mathrm{C^{18}O}$. While any estimates of line-of-sight locations

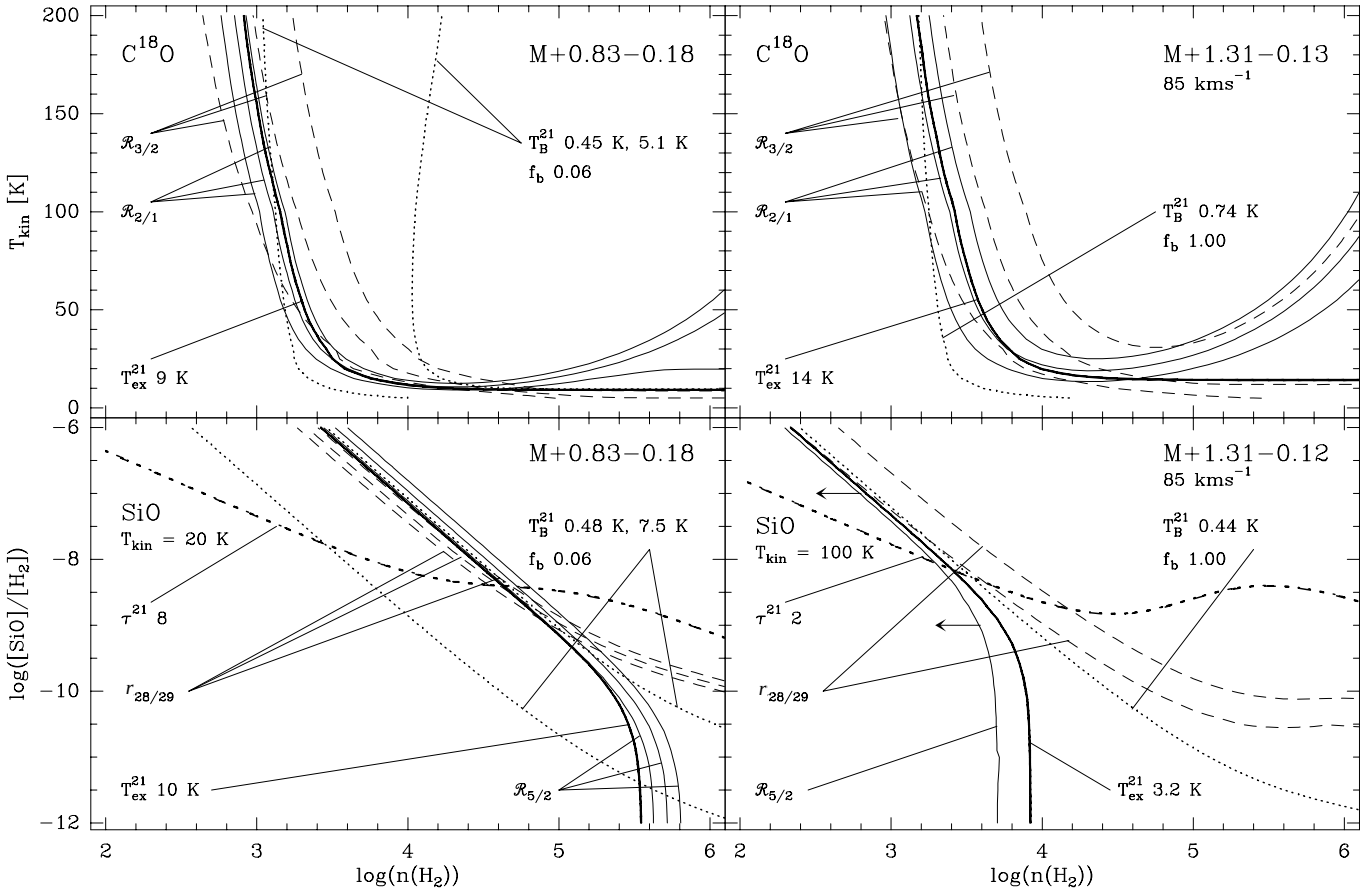

Fig. 3. LVG Model calculations for two individual sources, demonstrating the range of physical conditions encountered. The observed line intensity ratios are plotted including their 1 σ uncertainties. The $T_{\rm B}$- curves are the observed $T_{\rm MB}$ and the best fit temperature derived from the line ratios. The coresponding beam filling factor $f_{\rm b}$ is also given. For M+1.31–0.13, the observed and the best fit temperature are the same, thus $f_{\rm b} = 1$. τ^{21} is the peak optical depth of the ^{28}SiO line (not beam averaged).

in the Galactic center are rather uncertain, this plot gives a measure of location.

There is a clear trend in the large-scale distribution of SiO abundances. For $-0\overset{\circ}{.}35 \leq l \leq 0\overset{\circ}{.}6$, between the location of the Sgr C and Sgr B2 regions, we find a pronounced lack of very large X(SiO). Most clouds with very high abundances, including the exceptional source M+1.31–0.13, are located at $l > 0\overset{\circ}{.}8$. The 'Clump 2' Region is not included in this plot, since, at $l \approx 3^\circ$, this is not really part of the continuous molecular bulge or, in the notation of Morris & Serabyn (1996), the Central Molecular Zone (CMZ), although it shares many characteristics of the Galactic center gas. $X^{\rm SiO}$ in this region ranges from 1 10^{-9} to 2 10^{-9}, typical 'Galactic center' values that are high compared to the disk but not as extreme as what is found at $0\overset{\circ}{.}8 < l < 1\overset{\circ}{.}5$.

The detection of an 'SiO hole' at $-0\overset{\circ}{.}35 \leq l \leq 0\overset{\circ}{.}6$ is confirmed by an extension of the survey of Martín-Pintado et al. (1997) (unpublished data).

In recent years, the large scale dynamics of the gas in the CMZ, characterized by large non-circular motions and a distinct 'parallelogram' shape of lv-diagrams based on ^{12}CO and ^{13}CO (e.g. Bally et al. 1988), have been explained in terms of a model involving a rotating (stellar) bar with corotation at 2.4 kpc and oriented at an angle of $\sim 20^\circ$ with the line of sight to the Galactic center (see Morris & Serabyn 1996 and references therein). Within such a potential, there exist two categories of closed elliptical orbits, called x_1 and x_2-type orbits. Inside a cusped orbit, the x_1-orbits, which are elongated along the bar axis, become self-intersecting. Clouds on these orbits encounter a shock and within a dynamical time plunge into x_2-orbits that lie considerably deeper within the potential and mimic circular orbits (Mulder & Liem 1986, Athanassoula 1988, 1992). This encounter breaks the flow along the cusped orbit into a spray that spreads out into the interior of the orbit (Binney et al. 1991, Athanassoula 1992, Jenkins & Binney 1994).

According to this model, Sgr B2 and Sgr C can be interpreted to be at the locations of the intersections of the x_1- and the x_2-orbits. The dense, virialized clouds on the x_2-orbits, inside of Sgr B2 and Sgr C, are more likely to form stars, while the less dense clouds on the x_1 orbits are too disrupted by shocks for efficient star formation. Generally, this is supported by the fact that stars of young and intermediate age are restricted to the area inside of Sgr B2 and Sgr C, suggesting sustained star formation in this region (Serabyn & Morris 1996). In Sgr B2, the

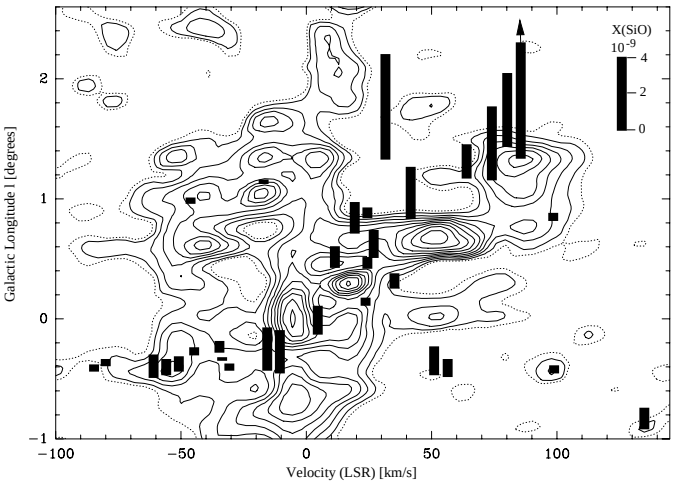

Fig. 4. The beam averaged SiO abundance plotted on a longitude-velocity diagram of the large scale distribution of $C^{18}O$, adapted from Paper I (spatial resolution $9'$).

ongoing star formation, the large amount of molecular gas, the existence of a very hot molecular component (Hüttemeister et al. 1993a, 1995, Flower et al. 1995) and the high optical depth of the ^{12}CO emission (Paper II) also provide ample evidence for this picture. The Sgr C complex is a much more quiescent region, but it contains a large H II region and GMCs.

Because the sprayed gas crashes into material that is still on x_1-orbits, collision regions are expected along the acceleration part of the cusped orbits. Due to perspective, these main collision areas should be at higher positive longitudes than Sgr B2 and between Sgr A and Sgr C. While the situation at negative l is confused (the gas on x_2 orbits and the collision regions are expected at similar Galactic longitudes), at positive l, especially the '$1\overset{\circ}{.}5$–complex' (Bally et al. 1988) shows all characteristics expected from a collision region (see the discussion in Paper II).

Inspecting Fig. 4 with this picture in mind, we find remarkable support from our data. The exceptional cloud M+1.31–0.13 and three other sources with high SiO abundances are located within the 1.5°–complex, exactly where strong shocks are expected. Generally, the high SiO abundances at $l > 0\overset{\circ}{.}8$ can be identified with a region in which the probability of gas encountering shocks is high. Thus, for the first time, we can tie the physical and chemical parameters of Galactic center molecular peaks to the large scale dynamics of the region.

Since CS traces all dense gas, not just the part that has been subjected to shocks, we do not expect a similar 'zone of avoidance'. Indeed, a plot similar to Fig 4 comparing the CS abundance in these clouds (data presented in Hüttemeister 1993), to the total H_2 column density does not show such an effect.

Of course, the correspondence is not absolute. Not every cloud at $l > 0\overset{\circ}{.}8$ *must* experience strong shocks. Note, however, that the clouds with very low SiO abundances in this range of l have negative velocities and might not be located in the collision region. Also, there are certainly strong shocks occuring in the Galactic center that are unrelated to large scale dynamics. Martín-Pintado et al. (1997) explain the 'SiO clouds' they find by shocks of a variety of origins: Interaction with SNRs close to Sgr A, interaction with non-thermal filaments in the radio arc and cloud-cloud collisions (as expected from large scale dynamics) or expanding bubbles in the vicinity of Sgr B2. Their map extends from $-0\overset{\circ}{.}2$ to $+0\overset{\circ}{.}8$. Therefore, they have missed the systematic signature of large scale effects present at higher positive longitudes.

Another mechanism explaining the preferential occurence of shocks in the $1\overset{\circ}{.}5$–complex might be fossil superbubbles, remnants of a phase of Sgr B2 type star formation activity. The expansion of superbubbles would offer a natural explanation of the large extent of the CO emission to positive Galactic latitudes perpendicular to the Glactic plane seen in this region. However, while the bar model as outlined above is two-dimensional and thus does not naturally produce vertical structure, sprayed gas colliding with gas on x_1-orbits might give rise to turbulence also pushing gas out of the plane. It is noteworthy that a ^{12}CO map (see, e.g., Paper II and Bitran et al. 1997) shows the molecular gas extending toward negative b at the southern edge of the CMZ. Thus, it seems possible that the CMZ is warped or susceptible to instabilities close to its edges (Morris & Serabyn 1996 and references therein).

The 'bar model' is not the only possibility to explain the large scale dynamics of the Galactic center region. von Linden et al. (1993) suggest that an accretion disk can also reproduce the basic structure seen in position-velocity plots. While this is certainly true for the inner region (x_2-orbits are almost indistinguishable from circular orbits) it is not clear whether such a scenario can also explain the gas distribution and the different chemical properties in the entire CMZ. Based on the data presented in Papers I and II and this work, we will examine the questions related to large scale structure and dynamics closely in a forthcoming paper (von Linden et al. 1998).

5.2. The origin of SiO

Even though the SiO emission we observe is mostly associated with cool gas, we consider it likely that it forms under conditions of high kinetic temperature and grain erosion by shocks (Martín-Pintado et al. 1992). Both the distribution discussed in the previous section and the existence of the hot cloud core M+1.31–0.13 can be taken as evidence for this. From the fact that only one cloud in our sample, namely M+1.31–0.13, shows hot gas emitting in SiO lines, we can conclude that shocked gas forms dense, cooler cores fairly fast. Extrapolating from the analysis in Hollenbach (1988), we find a very short cooling time scale ($\ll 10^6$ yr) for gas at a density of 10^4 cm^{-3}. A competing process is the condensation of gas phase SiO onto grain mantles. We estimate this 'freeze out' time scale to be of order 10^6 yr or slightly less (Rohlfs & Wilson 1996). Thus, gas with a high gas phase relative abundance of SiO has been cool for most of its lifetime.

After more than 10^6 years, the gas slowly loses the chemical memory of having been shocked. From the typical radial velocities of the clouds, we estimate that, during this time, these can move ~ 50 pc. If the very SiO-rich clouds are preferentially lo-

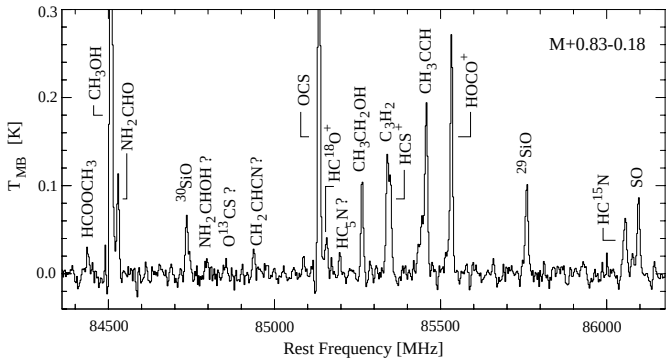

Fig. 5. The chemical complexity of sources strong in SiO is demonstrated by our spectrum of M+0.83–0.18, covering $\sim$ 1.8 GHz and including both ^{29}SiO and ^{30}SiO. The spectrum shown is a composite of two single SEST low frequency resolution spectra.

cated on x_1-orbits along the bar, these will remain sufficiently close in longitude to the region where they encountered the shock to be recognised as a distinct population.

Since we find some SiO in all cloud cores, additional formation of gas phase SiO is required, probably by local turbulence and/or cloud-cloud collisions causing some shocks. This is a general characteristic of the cores of Galactic center GMCs. Ongoing local shock activity is likely to be also necessary as the main heating mechanism for the hot gas component seen in all clouds (see Flower et al. 1995 and the discussion in Hüttemeister et al. 1993).

It is known that gas in post-shock regions, away from chemical equilibrium, is characterized by abundant complex molecules (e.g. Brown et al. 1988). This is exactly what can be observed toward the positions within the CMZ that are strong in SiO. We show just one example in Fig. 5. In the Galactic disk, such complex spectra are typical for very confined regions, while in the CMZ they seem to be ubiquitous. This chemical complexity can only be maintained for $\sim 10^6$ years and thus requires frequent shocks. These may also be typical for the starburst environment (see Henkel et al. 1987, Mauersberger & Henkel (1991), Mauersberger et al. 1991, Hüttemeister et al. 1997 for the case of NGC 253). On larger timescales, an equilibrium state is reached. This consists of a gas phase component of mostly diatomic molecules (Herbst & Leung 1989).

Most time-dependent chemical models have been calculated for either cold, quiescent clouds (e.g. Bergin et al. 1995) or 'classical' collapsing, star-forming hot cores (e.g. Brown et al. 1988, Caselli et al. 1993). Thus, detailed, model-supported recommendations of the molecules that should be used in future work to trace the chemical evolution of the the Galactic center cores cannot be given. CH_3OH and SO_2 appaer, however, to be promising species. The former is a high temperature, high density tracer requiring $T_{\rm kin} > 70$ K to evaporate from dust grains. Its wealth of emission lines allows density and temperature determinations from multi-level studies. Observations in external galaxies show that its abundance can differ widely even in the central regions of galaxies (Hüttemeister et al. 1997). SO_2 is associated with shock chemistry and grain destruction. The abundance of the two molecules need not be correlated, as is shown by an evolutionary study of cores in the W3 region (Helmich et al. 1994). Both molecules have lines that are strong enough to allow large scale mapping in the Galactic center region, and differences in their distribution would give further insight into the predominant processes operating on the Galactic center cores.

6. Conclusions

Based on our measurements and analysis of 33 molecular density peaks in the Galactic center in the $J = 1 \rightarrow 0, 2 \rightarrow 1$ and $3 \rightarrow 2$ transitions of $C^{18}O$, the $J = 2 \rightarrow 1$ and $5 \rightarrow 4$ transitions of ^{28}SiO and the $J = 2 \rightarrow 1$ transitions of ^{29}SiO and ^{30}SiO, we find:

1. All sources are easily detected in all transitions of $C^{18}O$ searched for and in ^{28}SiO($2 \rightarrow 1$), demonstrating that the properties of molecular peaks in the Galactic center region are markedly different from the Galactic disk, where thermal SiO emission is confined to very small regions in the vicinity of outflows associated with star formation. Local gas on the line-of-sight, distinguished from Galactic center gas by its narrow lines, is not detected in SiO.
2. The rare isotopomers ^{29}SiO and ^{30}SiO are detected in all 12 studied sources. The $J = 5 \rightarrow 4$ transition of the main isotopomers is seen in 7 out of 8 sources. The line intensity ratio of ^{29}SiO and ^{30}SiO shows that the terrestrial isotope ratio, ^{29}Si/^{30}Si = 1.5, holds for the Galactic center region.
3. From LVG model calculations applied to the $C^{18}O$ line intensity ratios $\mathcal{R}_{2/1}^{C^{18}O}$ and $\mathcal{R}_{3/2}^{C^{18}O}$, cool ($T_{\rm kin} \sim 20 - 30$ K) gas toward the molecular peaks has moderately high densities ($n\,(H_2) \sim (1-4)\,10^4$ cm^{-3}), while high kinetic temperatures of > 100 K correspond to H_2 densities that are an order of magnitude lower. This is contrary to what is found in the disk, where the cores of GMCs are usually hot, and is an indication that the 'cool cores' in 'typical' Galactic center GMCs, away from Sgr A and Sgr B2, are not presently forming high mass stars.
4. Combining the results of LVG models for $C^{18}O$ and SiO, and using $C^{18}O$ as a tracer of total H_2 column density, a beam averaged SiO abundance is derived for all clouds. This varies significantly from source to source, ranging from $\sim 0.3\,10^{-9}$ to $> 5\,10^{-9}$. The ^{28}SiO($2 \rightarrow 1$) transitions are optically thick, with τ_0 ranging from $2 - 8$.
5. Including information on the temperature structure of the clouds from NH_3, it is shown that for most clouds a self-consistent solution accounting for the properties of $C^{18}O$ and SiO is only possible if the bulk of the SiO emission arises in the cool, dense gas component.
6. One source, M+1.31−0.13, is different from all the others: SiO arises in the hot, thin gas component. Since this is also the cloud with the highest SiO abundance in the entire sample, the SiO formation process, probably grain erosion by shocks, is likely to be still ongoing in this source.
7. The SiO abundance in individual clouds is related to the large scale gas dynamics in the Galactic center region.

The highest abundances are found at Galactic longitudes of $l > 0.8°$, which can be identified with 'collision regions' likely to encounter shocks in terms of the bar model of gas dynamics.

8. As in the disk, SiO in the Galactic center region is likely to originate in shocks. Since the hot, thin post-shock gas forms dense, cool cores faster than SiO recondenses to dust grains, the SiO rich gas is cool for most of its lifetime. On a timescale of $\sim 10^6$ yr, the SiO molecules freeze out on grain mantles and the clouds lose their chemical memory of the shock.

Acknowledgements. We thank the staff of the telescopes, especially L. Knee and L.-Å. Nyman (SEST), and the SMTO/HHT staff for their help in taking the observations. GD gratefully acknowledges fiancial support from the Particle Physics and Astronomy Research Council (PPARC) (UK), for the observing run at JCMT. RM was supported by a Heisenberg fellowship by the Deutsche Forschungsgemeinschaft. JM-P has been partially supported by the Spanish DGES under grant number PB96-0104.

References

Athanassoula, E., 1988, Gas Flow in and around Bars; in T.D. Guyenne, J.J. Hunt (eds.), Plasma Astrophysics, Proceedings of the Joint Varenna-Abastumani International School and Workshop, ESA SP-285, Vol. I, p. 341
Athanassoula E., 1992, MNRAS 259, 345
Bally J., Stark A.A., Wilson R.W., Henkel C., 1987, ApJS 65, 13
Bally J., Stark A.A., Wilson R.W., Henkel C.,1988, ApJ 324, 223
Bania T.M., 1977, ApJ 216, 381
Binney J., Gerhard O.E., Stark A.A., Bally J., Uchida K.I., 1991, MNRAS 252, 210
Bergin E.A., Langer W., Goldsmith P.F., 1995, ApJ 441, 222
Bitran M., Alvarez H., Bronfman L., May J., Thaddeus P., 1997, A&AS 125, 99
Blake G.A., Sutton E.C., Masson C.R., Phillips T.G., 1987, ApJ 315, 621
Brown P.D., Charnley S.B., Millar T.J., 1988, MNRAS 231, 409
Caselli P., Hasegawa T.L., Herbst E., 1993, ApJ 408, 548
Cox P., Laurijs R., 1989, in: IAU Symposium 136: The Center of the Galaxy, M. Morris, (ed.), p. 121
Dahmen G., Hüttemeister S., Wilson. T.L., Mauersberger R., et al., 1997, A&AS 126, 197 (Paper I)
Dahmen G., Hüttemeister S., Wilson T.L., Mauersberger, R., 1998, A&A 331, 959 (Paper II)
de Jong T., Chu S.I., Dalgarno A., 1975, ApJS 199, 69
Downes D., 1989, Radio Astronomy Techniques, in: Evolution of Galaxies Astronomical Observations, Appenzeller I, Habing H.J., Léna P. (eds), Lecture Notes in Physics 333, 351
Duvert G., Cernicharo J., Baudry A., 1986, A&A 164, 349
Flower, D.R., Pineau des Forêts, G., Walmsley, C.M., 1995, A&A 294, 814
Farquhar P.R.A., Millar T.J., Herbst E., 1994, MNRAS 269, 641
Frerking M.A., Langer W.D., Wilson R.W., 1982, ApJ 262, 590
Genzel R., 1992, Physics and Chemistry of Molecular Clouds, in: The Galactic Interstellar Medium, Burton W.B., Elmegren B.G., Genzel R. (eds.), Saas Fee Advanced Course 21, 275
Green S., Chapman S., 1978, ApJS 37, 169
Güsten R., 1989, in: IAU Symposium 136: The Center of the Galaxy, M. Morris, ed., p. 89
Heiligman G.M., 1987, ApJ 314, 747
Helmich F.P., Jansen D.J., de Graauw Th., et al., 1994, A&A 283, 626
Henkel C., Walmsley C.M., Wilson T.L, 1980, A&A 82, 41
Henkel C., Jacq T., Mauersberger R., et al., 1987, A&A 188, L1
Herbst E., Leung C.M., 1989, ApJS 69, 271
Hollenbach D., 1988, Astro.Letters and Comm. 26, 191
Hüttemeister S., 1993, Dissertation, Bonn University
Hüttemeister S., Wilson T.L., Henkel C., Mauersberger R., 1993a, A&A 276, 445
Hüttemeister S. Wilson T.L. Bania T.M. Martín-Pintado J., 1993b, A&A 280, 25
Hüttemeister S, Wilson T.L. Mauersberger R. et al., 1995, A&A 294, 667
Hüttemeister S., Mauersberger R., Henkel C., 1997, A&A, 326 59
Jackson J.M., Heyer M.H., Paglione T.A.D., Bolatto A.D., 1996, ApJ 456, L91
Jenkins A., Binney J., 1994, MNRAS 270, 703
Langer W.D., Glassgold A.E., 1990, ApJ 352, 121
Lindquist M, Sandquist A., Winnberg A., Johansson L.E.B., Nyman L.-Å., 1995, A&AS 113, 257
Martín-Pintado J., Bachiller R., Fuente A., 1992, A&A 254, 315
Martín-Pintado J., de Vicente P., Fuente A., Planesas P., 1997, ApJ 482, L45
Mauersberger R., Henkel C., 1991, A&A 245, 457
Mauersberger R., Henkel C., Walmsley C.M., Sage L.J., 1991, A&A 247, 307
Mauersberger R., Wilson T.L., Mezger P.G., et al., 1992, A&A 256, 640
Mezger P.G., Duschl W.J., Zylka R., 1996, A&AR 7, 289
Morris M., Serabyn E., 1996, ARA&A 34, 645
Mulder W.A., Liem B.T., 1986, A&A 157, 148
Nakagawa T., Doi Y., Yamashita Y., et al., 1995 ApJ 435, L35
Odenwald S.F., Fazio G.G., 1984, ApJ 283, 601
Oka T., Hasegawa T., Hayashi M. et al., 1998, ApJ 493, 730
Penzias A.A., 1981, ApJ 249, 513
Rohlfs K., Wilson T.L., 1996, Tools of Radio Astronomy, 2nd ed., Springer, Berlin – Heidelberg
Scoville N.Z., Solomon P.M., 1974, ApJ 187, L67
Serabyn, E., Morris, M., 1996, Nature 382, 602
Stark A.A., Bania, T.M., 1986, ApJ 306, L17
von Linden S., Duschl W.J., Biermann P.L., 1993, A&A 269, 169
von Linden S., Hüttemeister S., Dahmen G., Duschl W.J., 1998, in prep.
White, R.E., 1977, ApJ 211, 744
Wilson T.L., Matteucci F., 1992, A&AR 4, 1
Wilson T.L., Rood R.T., 1994, ARAA 32, 191
Ziurys L.M., Friberg P., Irvine W.M., 1989, ApJ 313, 201